Int. J. Nanosci. Nanotechnol., Vol. 12, No. 2, June 2016, pp. 79-90

Detection of Polymer Brushes developed via Single Crystal Growth

S. Agbolaghi*, S. Abbaspoor and F. Abbasi

Institute of Polymeric Materials and Faculty of Polymer Engineering, Sahand University of Technology, Tabriz, Iran

(*) Corresponding author: s_agbolaghi@sut.ac.ir
(Received: 24 July 2014 and Accepted: 21 February 2016)

Abstract

Single crystals consisting various surface morphologies and epitaxial structures were applied to investigate the effect of other phase regions in the vicinity of a given tethered chains-covered area having a certain molecular weight of amorphous brushes. The designed experiments demonstrated that regardless of the type of surface morphology (patterned and especial mixed-brushes, homo and copolymer single-co-crystals or homo-brush single crystals and epitaxial structures), for a phase region covered by a certain type of brushes, the respective characteristics were similar. Detection of participating phases was possible by atomic force microscopy (AFM) on the basis of quality of employed solvent (amyl acetate) in growth systems, interaction of brushes with respective substrate, stiffness, and crystallinity of PEG-formed areas; hence, fabricated surfaces were not in need of any selective solvent to be detected. Moreover, structure of various single crystals was investigated by the help of conjunction thickness.

Keywords: *Epitaxial, Mixed-brush, PEG, Single-co-crystal, Single crystal.*

1. INTRODUCTION

Properties of the surface or interface modified by the polymer brushes can be significantly changed resulting in a wide range of applications of polymer brushes in various fields, consisting hydrogels, thin film stability, and environmentally sensitive controllers (chemical gates) [1-4]. To tether chains to substrates, several methods have been proposed via *physical adsorption* or *chemical grafting* of chains onto substrates via *grafting to* [5-7] or *grafting from* [8-10] techniques. Living free radical polymerization was also used for hyperbranched grafting of the copolymers [11].

The third method called *single crystal growth* [12,13], which is able to produce the homogeneous distribution and brush length and to adjust accurate grafting density, has priority to others [12,14]. A single-co-crystal is a uniform or non-uniform crystalline structure composed of two or more crystallizable constituents [15]. To obtain a combination of various properties for a surface-grafted monolayer, the polymer mixed-brushes could be fabricated. It is noteworthy that due to presence of different polymer brushes having various behaviors in mixed-brush structures, they are capable to introduce a wide range of morphologies as well as responses [16-18].

Mixed-brushes could be fabricated by grafting to, grafting from, combination of both, single crystal growth of star block copolymers, and the novel approach introduced recently by our research group entitled *single crystal surface patterning* having unique properties, in which the single crystals were grown from dilute solution including two different types of

crystalline-amorphous diblock copolymer chains with the same crystalline block [18]. The detection of PS-*b*-PMMA diblock brushes on the surface of the crystalline poly(L-lactide) (PLLA) required some selective solvents [14]. However, the patterned leopard skin-like surface morphologies were independent of any selective solvent to be detected [18]. Another issue settled by our group in this field was study of various developed surface morphologies of *single-co-crystals* grown from homo and diblock copolymer chains (PEG-*b*-PS/PEG and PEG-*b*-PMMA/PEG) [15]. We also have worked on *nascent lateral habits* for solution crystallization of PEG-*b*-PS diblock copolymers [19]. Meanwhile, construction of *epitaxial nanostructures* from various amorphous-crystalline diblock copolymers including PEG-*b*-PS, PEG-*b*-PMMA, and homo-PEG chains which had the same crystalline block has been covered by our group. In addition to verify the corresponding thickness of substrate in different phase regions of single crystals with mixed-brush surface morphologies, the channel-wire arrays have been employed to investigate the chemical and geometric recognition applications [20].

In addition, there is a limited literature on the polymer semiconductor single crystals or highly crystalline self-assembled nanostructures, e.g., poly (3-hexylthiophene) (P3HT) [21], poly(3-butylthiophene)-*b*-Poly(ethylene) (P3BT-*b*-PE) [22], and PANI-*b*-PEG-*b*-PANI [23,24].

2. EXPERIMENTAL

Demanded materials including PEG-*b*-PS and PEG-*b*-PMMA with the same molecular weight of crystalline block and different molecular weights of amorphous blocks were synthesized via atom transfer radical polymerization (ATRP). Detailed synthesis procedures were described elsewhere [18].

The corresponding PDIs for PEG-*b*-PS and PEG-*b*-PMMA were in the range of 1.13-1.16 and 1.19-1.21, respectively. The details of self-seeding technique used to grow the single crystals of diblock copolymers have been described elsewhere [25, 26]. Here, we have adopted this approach to grow the single crystals with various surface morphologies. Solution crystallization was carried out with a dilute concentration of 0.009 wt% for homopolymer and homo-brush, and 0.018 wt% (wt/wt of PEG-*b*-PS/PEG-*b*-PMMA was 50/50) for mixed-brush and homo and copolymer single-co-crystals in amyl acetate (Merck, > 98%). Four stages of the employed technique were reported in details elsewhere [15, 18, 20, 27].

^{1}H NMR spectra were recorded on a Bruker (Avance DPX) spectrometer at frequency of 400 MHz to determine the chemical structure and the composition of the copolymers. Deuterated chloroform ($CDCl_3$) was used as a solvent. The polydispersity indexes were determined by GPC on a WATER 1515 (USA) gel permeation chromatography instrument with a set of HT3, HT4, and HT5, μ-styragel columns with DMF and THF as eluents (1.0 mL/min) for PS and PMMA, respectively, at 35 °C. Some monodisperse polystyrene standards were utilized for calibration.

In order to measure the glass transition temperature (T_g) and crystallization temperature (T_c) of synthesized diblock copolymers differential scanning calorimetry (DSC) (NETZSCH, F3 Maia200) was utilized.

To measure the overall single crystal thickness and identify their surface morphologies, an atomic force microscope (AFM, Nanoscope IIIA) was employed. Some research groups have focused on the configuration of AFM instrument [28,29].

Single crystal morphology was observed in a transmission electron microscope (TEM, EM 208 Philips) with an accelerating voltage of 100 KeV. The selected area electron diffraction (SAED) were also conducted to determine the chain orientation in the copolymer single

crystals.

3. RESULTS AND DISCUSSION

Figure 1 illustrates the ^{1}HNMR spectra of PEG_{5000}-*b*-PS_{4600} and PEG_{5000}-*b*-$PMMA_{13100}$ block copolymers. In this work, the constituents of single crystals were crystalline homo and crystalline-amorphous block copolymers. Figure 2(a) depicts the GPC traces of synthesized block copolymers through different graphs comprising PEG_{5000}-*b*-PS_{4600} (a), PEG_{5000}-*b*-$PMMA_{8700}$ (b), PEG_{5000}-*b*-PS_{10000} (c), PEG_{5000}-*b*-$PMMA_{13100}$ (d) and PEG_{5000}-*b*-PS_{14800} (e).

Figure 2(b, left) reports the DSC heating and cooling cycles with the scanning rate of 5 K/min for collected mats of homo-PEG_{5000} single crystals. Similarly, Figure 2(b, right) represents T_m and T_g of the bulk of PEG_{5000}-*b*-PS_{14800} block copolymers with the scanning rate of 5 K/min.

Figure 3(a), (b), and (c) illustrate the height image, phase image and height profile of leopard skin-like mixed-brush single crystal of PEG_{5000}-*b*-PS_{4600}/PEG_{5000}-*b*-$PMMA_{8700}$ grown at T_c = 30 °C, respectively. Related height variance and domain size were 4.70 and 348 nm, respectively. This patterned surface morphology for polymer mixed-brushes could be ascribed to two main reasons.

First, the conformations of PS and PMMA amorphous blocks are different in amyl acetate, which is a partially poor and a very good solvent for PMMA and PS blocks, respectively [12, 13, 30, 31]. Hence, the PS chains are more extended in comparison to the PMMA ones. The mentioned conformation of PS blocks may cause them to be included into the single crystal structure more conveniently, and upon absorbing the primary PEG-*b*-PS chain into the single crystal structure, the tendency towards the chains having the same type of amorphous blocks, due to more stretched conformation of the PS chains at growth condition, is higher in comparison to the others. That is why, the latter polymer chains included in the structure are of the same sort and, consequently, the surface areas covered by PS tethered chains form the matrix phase.

Second, the interaction of substrate surface with PMMA and PS grafted chains are of the sort of attraction and repulsion, respectively. Therefore, the grafted PMMA chains tend to be attracted to the substrate surface and, subsequently, increase the segmental density in the vicinity of it; on the contrary, the PS ones like to be repulsed from the surface and reach to the more extended conformations. The PMMA chains had somewhat packed pancake shape conformation; so, their hindrance against the chains with the same blocks is significantly high; that is why, we speculate that due to higher hindrance of PMMA chains, which exert greater surface pressure on the substrate, the PEG-*b*-PS diblock copolymer chains have more opportunity to be included into the single crystal structure in comparison with the PEG-*b*-PMMA ones. Therefore, due to compatibility of PMMA chains with PEG crystalline blocks [32] and their more coily conformations, the PS brushes treat them like homo-PEG chains, so the chains in question are capable to enter into the single crystal structure.

Besides, for high hindrance of PMMA grafted chains, the phase regions constructed with them could only contribute to small spread patches. In conclusion, the matrix (PS)-dispersed (PMMA) surface morphology is substantiated for higher hindrance against PEG-*b*-PMMA chains to be entranced into the single crystal structure.

Regarding the densities of PMMA and PS amorphous blocks (= 1.19 g/cm^3 [31] and 1.05 g/cm^3 [33], respectively), it may be claimed that the stiffness of PMMA brushes is higher than that of PS ones. Therefore, AFM could be adopted to recognize differences. Microscopic speaking, the depth of a static indentation for an AFM tip penetrating into PS regions is approximately 5 nm while a tip penetrating into PMMA domains is less

than 1 nm [14]. So, the opaque phase regions in the role of dispersed domains could be ascribed to the surface areas covered by PMMA tethered chains. Third, the most influential parameter lies in the interaction between varying brushes of PMMA and PS with substrate. Moreover, due to higher osmotic pressure of PMMA chains [18], the substrate thickness under PMMA covered area is less than that of PS covered ones. The presented reasons can thus cause the conspicuous height variances between different PS-matrix and PMMA-dispersed phases.

To introduce the various surface morphologies in homo and copolymer single-co-crystal systems, it suffices to declare that the matrix (PS)-disperse (PEG), matrix (PMMA)-disperse (PEG), and matrix (PEG)-disperse (PMMA) morphologies have been recognized.

The matrix-disperse single-co-crystal of PEG_{5000}-*b*-PS_{4600}/PEG_{5000} (grown at T_c = 30 °C) having height variance (= 4.81 nm) and domain size (= 145 nm) and respective height profile are depicted in Figure 3(d) and (e), in respect. Although there was no tethered chains in PEG-dispersed phase region, the height variance was not significantly higher than that of PMMA-covered area in PEG_{5000}-*b*-PS_{4600}/PEG_{5000}-*b*-$PMMA_{8700}$ mixed-brush single crystal. It could be ascribed to highly packed pancake conformation of PMMA brushes on the single crystal substrate surface.

To explain quantitatively, the total thickness of PS-covered regions, which own the role of matrix, in both PEG_{5000}-*b*-PS_{4600}/PEG_{5000}-*b*-$PMMA_{8700}$ and PEG_{5000}-*b*-PS_{4600}/PEG_{5000} single crystals were equal to 16.10 and 16.13 nm, respectively, and the total thickness of PMMA- and PEG-disperse regions in these two systems were (= 11.40 and 11.32 nm), respectively. It is charming that the thickness of PMMA-covered areas does not have any conspicuous difference with bared-disperses of PEG chains.

Figure 3(f) and (g) show the height image and height profile of homo-brush single crystal of PEG_{5000}-*b*-PS_{4600} grown at T_c = 30 °C. Similarly, epitaxial structure single crystal of PEG_{5000}-*b*-$PMMA_{8700}$, PEG_{5000}-*b*-$PMMA_{8700}$/PEG_{5000}-*b*-PS_{4600}, homo-PEG_{5000}, PEG_{5000}-*b*-PS_{4600}, homo-PEG_{5000} grown at T_c = 30 °C and respective height profile are presented in Figure 3(h) and (i), respectively.

As a conclusion, regardless of the brushes in the vicinity of given phase region and their molecular weight as well as the type of surface morphology (i.e., being in homo and copolymer single-co-crystal, mixed-brush, epitaxial structure, homo-brush or homopolymer single crystal), the features like thicknesses were repeatable for a certain amorphous and crystalline blocks molecular weight.

Quantitatively speaking, the total thickness of phase regions covered by PS grafted chains in the patterned mixed-brush single crystal of PEG_{5000}-*b*-PS_{4600} (matrix)/PEG_{5000}-*b*-$PMMA_{8700}$ (dispersed), single-co-crystal of PEG_{5000}-*b*-PS_{4600} (matrix)/PEG_{5000} (dispersed), mixed-brush channel of epitaxially grown PEG_{5000}-*b*-PS_{4600} (matrix)/PEG_{5000}-*b*-$PMMA_{8700}$ (dispersed), homo-brush channel of epitaxially grown PEG_{5000}-*b*-PS_{4600}, and homo-brush single crystal of PEG_{5000}-*b*-PS_{4600} were 16.10, 16.13, 16.09, 16.10, and 16.11 nm, respectively.

Similarly, the total thickness of phase regions covered by PMMA grafted chains in the patterned mixed-brush single crystal of PEG_{5000}-*b*-PS_{4600} (matrix)/PEG_{5000}-*b*-$PMMA_{8700}$ (dispersed), mixed-brush channel of epitaxially grown PEG_{5000}-*b*-PS_{4600} (matrix)/PEG_{5000}-*b*-$PMMA_{8700}$ (dispersed), homo-brush channel of epitaxially grown PEG_{5000}-*b*-PS_{8700} were 11.40, 11.40, and 11.41 nm, respectively.

Subsequently, the thickness of bared substrate formed from PEG chains in the single-co-crystal of PEG_{5000}-*b*-PS_{4600} (matrix)/PEG_{5000} (dispersed) and homo-PEG_{5000} channels of epitaxial structure were equal to 11.32, 11.30, and 11.31 nm, respectively.

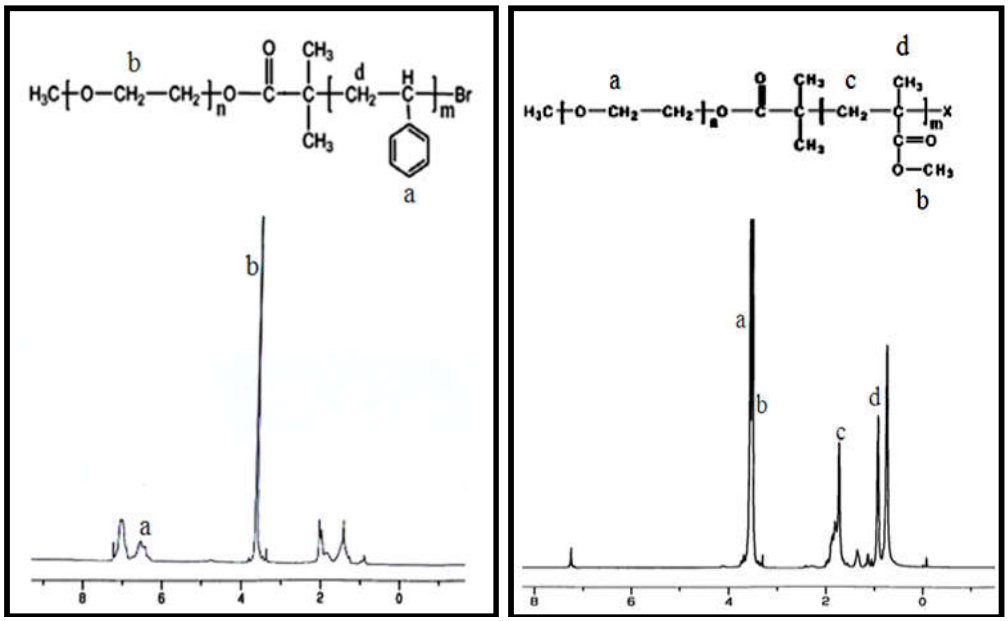

Figure 1. *[1]HNMR spectra of PEG_{5000}-b-PS_{4600} (left); PEG_{5000}-b-$PMMA_{13100}$ (right).*

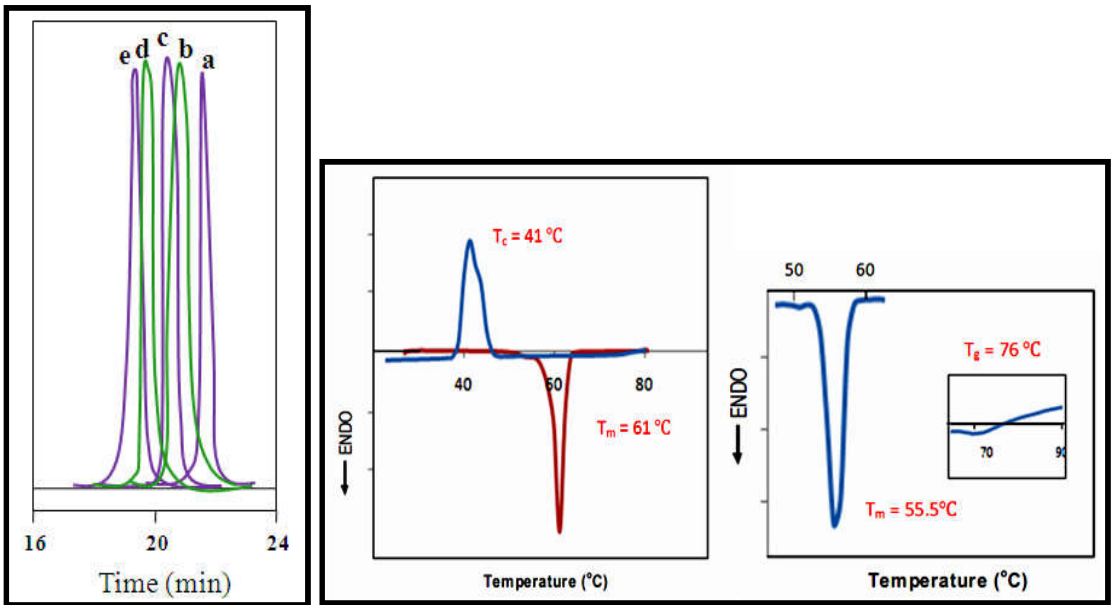

(a) (b)

Figure 2. *(a) Evolution of GPC traces of PEG_{5000}-b-PS_{4600} (a), PEG_{5000}-b-$PMMA_{8700}$ (b), PEG_{5000}-b-PS_{10000} (c), PEG_{5000}-b-$PMMA_{13100}$ (d), and PEG_{5000}-b-PS_{14800} (e); (b) DSC heating and cooling cycles with the scanning rate of 5 K/min for collected mats of homo-PEG_{5000} single crystals (left); determining T_m and T_g of the bulk of PEG_{5000}-b-PS_{14800} block copolymers with the scanning rate of 5 K/min (right).*

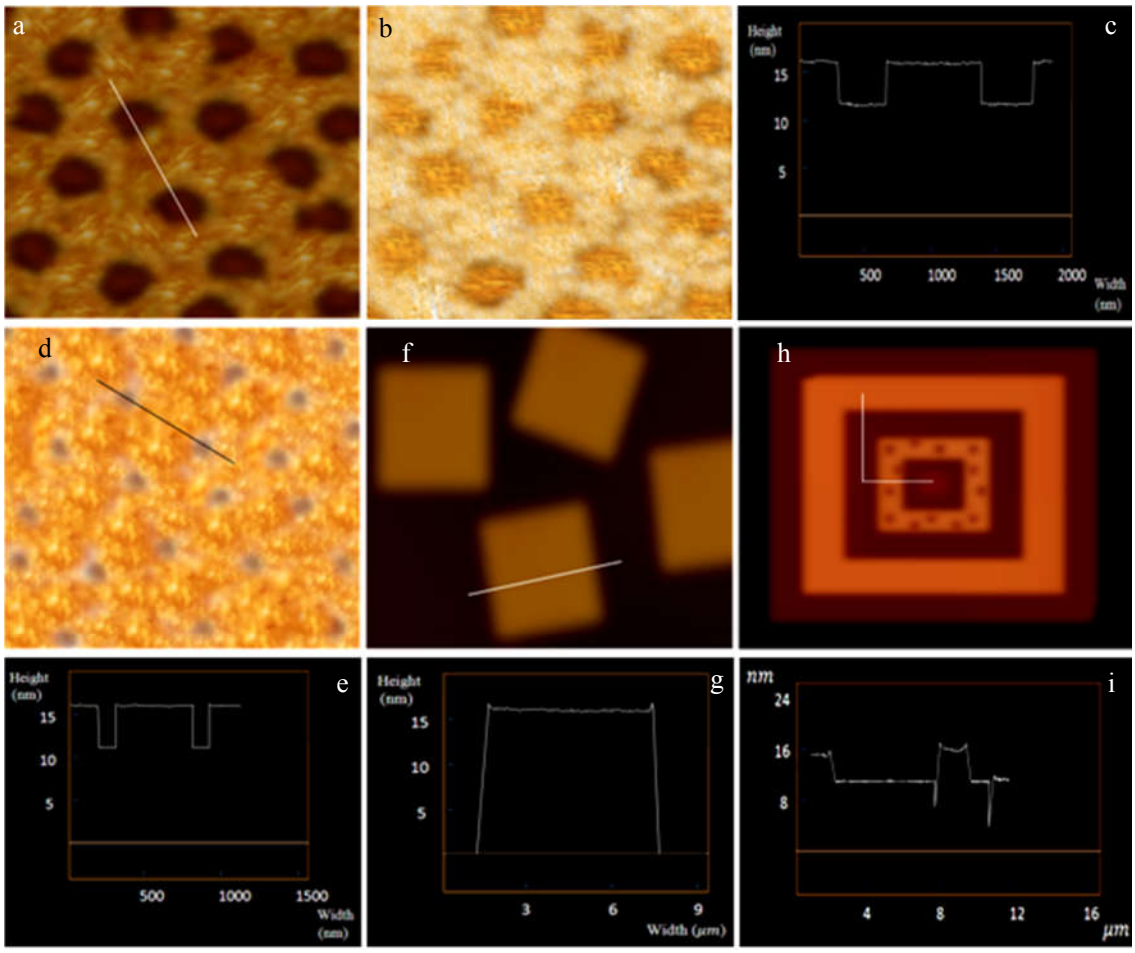

Figure 3. *AFM NanoscopeIII image of single crystals grown at T_c = 30 °C. Leopard skin-like mixed-brush single crystal of PEG_{5000}-b-PS_{4600}/PEG_{5000}-b-$PMMA_{8700}$, height image (the maximum z-scale is 5 nm), height variance: 4.70 nm, domain size: 348 nm (a), phase image (the maximum z-scale is 5°) (b), height profile (c); matrix-disperse single-co-crystal of PEG_{5000}-b-PS_{4600}/PEG_{5000}, height image (the maximum z-scale is 5 nm), height variance: 4.81 nm, domain size: 145 nm (d), height profile (e); homo-brush single crystal of PEG_{5000}-b-PS_{4600}, height image (f), height profile (g); single crystal having epitaxial structure of PEG_{5000}-b-$PMMA_{8700}$ (d^{total} = 11.41 nm) ⇒ homo-PEG_{5000} (d^{total} = 11.38 nm) (Junction point = 4.11 nm)⇒ PEG_{5000}-b-PS_{4600} (d^{total} = 16.09 nm)/PEG_{5000}-b-$PMMA_{8700}$ (d^{total} = 11.40 nm)(domain Size: 350 nm) ⇒ homo-PEG_{5000} (d^{total} = 11.30 nm) (Junction point= 7.65 nm) ⇒ PEG_{5000}-b-PS_{4600} (d^{total} = 16.10 nm) ⇒ homo-PEG_{5000} (d^{total} = 11.31 nm)) (Junction point = 7.85 nm) (h), height profile (i). The weight ratio of applied materials in mixed systems was 50/50 for cocrystallization.*

In either patterned mixed-brush single crystal of PEG_{5000}-*b*-PS_{4600}/PEG_{5000}-*b*-$PMMA_{8700}$ grown separately at T_c = 30 °C (Figure 3(a)) or the same mixed-brush developed as one of channels of an epitaxial structure in Figure 3(h), the As other examples, for leopard skin-like mixed-brush single crystal of PEG_{5000}-*b*-PS_{10000}/PEG_{5000}-*b*-$PMMA_{13100}$ grown at T_c = 23 °C, the total height of PS-matrix and domain size of PMMA-disperses was 348 and 350 nm, respectively. So, being confined as a channel in an epitaxial structure, does not affect the average domain size of disperses fabricated in a matrix with the same molecular weights.

PMMA-disperse were (= 16.42 and 11.20 nm), for single-co-crystal of PEG_{5000}-*b*-PS_{10000}/PEG_{5000} at the same growth condition, the PS-matrix and PEG-disperse were (= 16.32 and 10.26 nm), and similarly, for homo-PEG_{5000}, the total height of single crystal was (= 10.33). Drawing comparison between reported data, one can see that the percentage of adaptability was high enough to declare that the conducted experiments were repeatable, albeit with exerting scrutiny.

The tethering density and crystalline substrate thickness can be determined from Equations (1) and (2), respectively [12, 13, 30].

$$\sigma = \frac{1}{S} = \frac{1}{\frac{2M_n{}^{CRYST}}{N_A \rho_{CRYST} d_{CRYST}}} = \frac{N_A \rho_{CRYST} d_{CRYST}}{2M_n{}^{CRYST}} \quad (1)$$

$$d_{CRYST} = d^{total} \times \frac{M_n^{CRYST}/\rho_{CRYST}}{M_n^{CRYST}/\rho_{CRYST} + M_n^{AM}/\rho_{AM}} \quad (2)$$

where σ, N_A, ρ_{CRYST}, d_{CRYST}, $M_n{}^{CRYST}$, d^{total}, M_n^{AM}, and ρ_{AM} stand for the tethering density, the Avogadro number (= 6.022×10^{23} mol^{-1}), crystalline PEG density (is equal to 1.239 g/cm^3 at room temperature) [33], PEG substrate thickness (Eq (2)), the molecular weight of PEG (= 5000 g/cm^3 for all samples), the total thickness, the molecular weight of amorphous blocks, the density of amorphous blocks (1.19 g/cm^3 [31] for PMMA and 1.05 g/cm^3 [33] for PS), respectively.

Another issue which is supposed to be tackled here is conjunction thickness. Where in epitaxial structures, a brush-covered channel is next to a homopolymer single crystal channel, on the conjunction of these two channels one cannot determine the substrate thickness of latter channel; because when the substrate surface is covered by tethered chains, the junction point of two crystals in the vicinity of each other is not representative of second channel substrate thickness. As a regulation we did it reversely. We developed the homo-PEG single crystals next to the brush-covered channels to verify the substrate thickness out of conjunction thickness. It is noted that at the conjunction between diblock copolymer and homopolymer single crystals, the thickness has to be confined to the same thickness which is provided by previously presented growth fronts. However, the crystalline substrate thickness at the conjunction of corresponding diblock copolymer and homopolymer crystalline layers was equal to that of diblock copolymer single crystal. Because of the energetic contribution of amorphous chains in the diblock sample, the thermodynamic metastable thickness of these two types of crystals changed at the same crystallization temperature. As the crystal grows away from the seed, the thermodynamic thickness will be gained, which is larger than primary substrate thickness definitely. Therefore, the measurement of thickness at the conjunction of copolymer and homopolymer crystals could provide an accurate determination for the substrate thickness of copolymer single crystals [12, 13, 30]. Adopting the height profile of epitaxial structures obtained by means of AFM, and concerning the conjunction thickness between the corresponding copolymer and homopolymer crystals, which was achievable from the height profile, we were able to verify the calculated crystalline substrate thickness in single crystals with matrix-dispersed surface morphology [18]. It should be noted that in some cases of AFM analyses, while depositing the crystals onto a hard silicon wafer surfaces, the homo-PEG single crystals slipped down to the silicon surface for the gravity effect, as it can be seen in height profile of Figure 3(i). Here, the thicknesses achieved at the conjunctions of the copolymer seeds is a direct measure of the d^{PEG}. Avoiding the slippage of homo-PEG single crystal, height variance between the top surface of

the diblock copolymer and corresponding homo-PEG single crystal at the conjunction is thus equal to the d^{PS}. In this case, one should apply the relation of $d^{total} - 2d^{PS}$ to determine the d^{PEG} [13, 30]. The calculated substrate thicknesses of PMMA- and the PS-covered phase regions in mixed-brush single crystals were highly compatible with the achieved conjunction thicknesses from respective channels of epitaxial structures. As some instances, considering Figure 3(i) (height profile of epitaxial structure single crystal of PEG_{5000}-*b*-$PMMA_{8700}$,PEG_{5000}-*b*-$PMMA_{8700}$/PEG_{5000}-*b*-PS_{4600}, homo-PEG_{5000}, PEG_{5000}-*b*-PS_{4600}, homo-PEG_{5000}, respectively), it could be seen that the conjunction thickness in the boundary of PMMA-covered and bared-PEG channels is (= 4.11 nm), and it is highly adaptable with calculated thickness for PMMA-covered substrate in homo-brush PEG_{5000}-*b*-$PMMA_{8700}$ single crystal (= 4.06 nm). Similarly, the conjunction thickness in the boundary of PS-covered and bared-PEG channels is (= 7.65 nm), and it proves the corresponding substrate thickness in PS-matrix phase region of leopard skin-like mixed-brush single crystal of PEG_{5000}-*b*-PS_{4600}/PEG_{5000}-*b*-$PMMA_{8700}$ (= 7.72 nm), PS-matrix phase region in matrix-disperse single-co-crystal of PEG_{5000}-*b*-PS_{4600}/PEG_{5000} (= 7.73 nm), and PS-covered substrate in PEG_{5000}-*b*-PS_{4600} homo-brush single crystal (= 7.72 nm).

Beside patterned leopard skin-like surfaces, polymer mixed-brushes with especial surface morphologies were developed through growth of single crystals from dilute solution comprising PEG-*b*-PS and PEG-*b*-PMMA diblock copolymers. These morphologies, which were in minority in comparison to the ideal and predictable inside-filled matrix-disperse morphologies, divided into some categories: snake-, ring-, and dumbbell-like PMMA-disperses in PS-matrix, two-, three-, four-, five-, and six-patched surface areas covered by PS and PMMA grafted chains, and random channel-like morphologies with alternative channels constructed from two different phases. Irrespective of their unpredictable surfaces, their features including surface of various PS- and PMMA-covered phases, the total, substrate, and amorphous thickness resembled that of patterned morphologies having the same requisites. Furthermore, the surface morphology and amorphous blocks molecular weight were ineffective on crystalline structure of substrate and the dominant growth fronts of (120). The mentioned surface morphologies were detected like patterned morphologies.

In general, for single-co-crystals grown from homo and copolymer chains, there have been two types of surface morphologies fell into: random and matrix-disperse single-co-crystal. For growth systems, in which the height variance is considerable (especially matrix (PS)-dispersed (PEG)), the main effective parameter to detect the various phase regions is the height variance between appearanced phases. Nevertheless, for samples with insignificant height variance, the top notch parameter to analyze the phase regions is crystallinity of PEG-fabricated area as well as different amorphous and crystalline blocks density.

To explain in detail, in PEG-*b*-PMMA/PEG matrix-disperse single-co-crystals, either regions covered with tethered PMMA brushes or bared-substrate consisting homo-PEG chains form the matrix phase or vice versa, there existed some samples, while in which the height variance between different phases was very low (0.04-2.04 nm), due to two reasons presented below, the surface areas of homo-PEG chains (bared-area) were much opaque in comparison with the PMMA-covered regions. First, the density reported in references for PEG chains in crystalline state is to some extent greater than that of PMMA ones (1.24 g/cm^3 [33] vs 1.19 g/cm^3 [31]). Second, the PEG chains forming either matrix or disperse phase are included in crystalline structure

of substrate; so they have more packed and ordered arrangement in comparison to the amorphous PMMA attached regions, in which the chains have repulsive interaction with other chains located in their vicinity, consequently, they are reluctant to be in ordered arrangement. This is why their responses to the tip of AFM were different. Hence, despite low height variance, different phase regions were detectable. However, in PEG-*b*-PS/PEG matrix-disperse co-crystal growth systems, the height variance between matrix and disperse phases was high enough (3.63-10.30 nm). It is obvious that the height images obtained by means of AFM had more clarity and resolution definitely. Hence, the different phase regions were separated through two varying darker and lighter colors, in which darker areas belonged to the bared-substrate and lighter ones were covered with tethered brushes.

Besides, in matrix-disperse co-crystals made of either PEG-*b*-PMMA/PEG or PEG-*b*-PS/PEG chains, through enhancement of the amorphous block molecular weight, the height variance between matrix and disperse phase regions was elevated and, consequently, the clarity of images increased. Note that distinction of matrix and disperse phase regions through opacity and transparency is more useful for the samples, in which the height variance is not high enough, while for the samples having noticeable height variance, the color differences is much more beneficial.

The verification of random single-co-crystals whose surface morphologies resembled those of homo-brush single crystals, blanketed an important part of this research. Three approaches are presented here for doing so. First, the total thickness obtained by AFM was higher for random co-crystals in comparison to corresponding homo-brush single crystals. The height profiles associated with three sorts of single crystals crystallized at T_c = 23, 28 and 32 °C in dilute solution of amyl acetate including homopolymer of homo-PEG_{5000} (10.33, 11.09 and 11.55 nm), random co-crystal of PEG_{5000}-*b*-PS_{4600}/PEG_{5000} (16.12, 17.19 and 18.61 nm) and homo-brush of PEG_{5000}-*b*-PS_{4600} (13.96, 15.12 and 16.65 nm) proved this claim. The mentioned trend held truth for PMMA dealt systems as well. As an instance, the total thickness of single crystals grown at the same temperatures for homo-PEG_{5000}, random co-crystal of PEG_{5000}-*b*-$PMMA_{13100}$/PEG_{5000}, and homo-brush of PEG_{5000}-*b*-$PMMA_{13100}$ were 10.33, 15.52 and 11.33 nm, in respect.

Second, Comparing the central sphere of related TEM electron diffraction (ED) technique patterns for homo-PEG and homo-brush single crystals (Figure 4(a) and (c)), one could behold that the central sphere of samples comprising diblock copolymer chains is smaller than that of homopolymer crystal. We speculate that it could be related to higher order of homopolymer single crystals which do not have any disturbing amorphous brushes in their structure. Similarly, at the same growth condition, the size of central sphere for random co-crystals is greater in comparison with corresponding homo-brush single crystals, whereas it is smaller than that of respective homopolymer single crystals. It could be said that due to presence of homo-PEG chains which do not have any amorphous blocks in random co-crystals structure, their order is higher than that of corresponding homo-brush single crystals; hence, the central spot which belongs to random single-co-crystal is bigger than that of respective homo-brush one. On the other side, the structural order of homopolymer single crystals is in a high level in comparison to the random co-crystals. Therefore, the mentioned spot is smaller for latter ones. TEM bright images and ED patterns for grown single crystals in amyl acetate at T_c = 23 °C including homo-PEG_{5000}, random co-crystal of PEG_{5000}-*b*-PS_{10000}/PEG_{5000} and homo-brush of PEG_{5000}-*b*-PS_{10000} are depicted in Figure 4. Note that the ED

patterns of all samples possess four light spots entitled (120) around the central core which are representative of four dominant fronts filled with polymer chains and grown during the single crystal completion. These major fronts constitute four sides of square of ideal and monolayer single crystal; this is in accordance with those have been reported for homo-PEG and copolymer single crystals having PEG as crystalline substrate up to now [12,13,19,30]. Using a very weak spot, limited in size of only the crystal, and working in defocused diffraction pattern mode and, subsequently, taking quickly the DP, we were capable to record the weaker (200) and (110) spots which primarily were detected by Lotz [26].

We believe that this analysis will contribute to understanding of the polymer crystallization process at the molecular scale in co-crystallization systems and the interplay between the crystallizable and amorphous parts of the system during this process, in which the growth fronts are the same for homo PEG, homo-brush and co structured single crystals while the order level of crystalline structures are different.

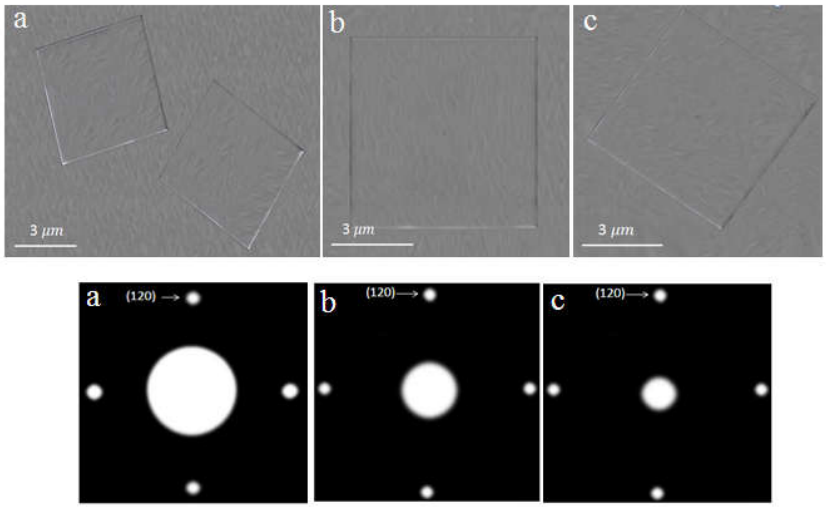

Figure 4. *TEM bright images (up) companied by corresponding ED patterns of the square-shaped single crystals (down) grown in amyl acetate at T_c = 23 °C; homo-PEG$_{5000}$ (a); random co-crystal of PEG$_{5000}$-b-PS$_{10000}$/PEG$_{5000}$ (b); homo-brush of PEG$_{5000}$-b-PS$_{10000}$ (c).*

Third, comparing the melting temperature (T_m) of mentioned three types of single crystals measured by means of DSC instrument is the last way. It is noteworthy that the presence of amorphous blocks in the single crystal structure can somehow decrease its T_m. Based on DSC analyses conducted on the collected mats of single crystals the trend of $T_{m(\text{homo-PEG})} > T_{m(\text{random co-crystal of PEG-}b\text{-PS(PMMA)/PEG})} > T_{m(\text{homo-brush of PEG-}b\text{-PS(PMMA)})}$ was detected. In single-co-crystal growth systems of PEG-*b*-PS/PEG, there were four various and, consequently, four different portions of amorphous blocks. Therefore, collecting the mats associated with random co-crystals is out of question. That is why we were not able to verify our samples through this proposed method.

Concerning the obtained data for PEG$_{5000}$-*b*-PS$_{14800}$ and PEG$_{5000}$-*b*-PMMA$_{8700}$ homo-brush single crystals and amyl acetate as a very good solvent for PS chains and a partially poor solvent for PMMA ones at growth condition, we concluded that R_g of PMMA in PEG$_{5000}$-*b*-PMMA$_{8700}$ was less than that of PS in PEG$_{5000}$-*b*-PS$_{14800}$. For to an extent the same molecular weights of PS and PMMA blocks, the gyration radius of PS in amyl acetate as a very good

solvent is 3.7 nm, whereas the gyration radius in the same solvent for PMMA as a partially good solvent is 3.4 nm. In our systems the most effective parameter on the substrate thickness can be ascribed to the interaction between tethered brushes and substrate surface. The mentioned trend has been satisfied at elevated crystallization temperature as well.

In addition to all introduced surface morphologies for single-co-crystal growth systems from homo and copolymer diblock copolymers, some structures were observed in which neither the spread patches were big enough to be detectable nor the respective thicknesses were high enough to be considered a random single-co-crystal. The detection of structures in question resembled that of random single-co-crystals.

4. CONCLUSION

Various surface morphologies were developed from dilute solutions of solutes in amyl acetate. Irrespective of the brushes in the vicinity of given phase region and their molecular weight as well as the type of surface morphology, the features such as thickness was repeatable for a certain amorphous and crystalline blocks molecular weight. Furthermore, the homo-PEG single crystals were developed next to the brush-cover channels to verify the substrate thickness of different morphologies on the basis of conjunction thickness

REFERENCES

1. Ohsedo, Y., Takashina, R., Gong, J. P., Osada, Y., (2004). "Surface friction of hydrogels with well-defined polyelectrolyte brushes," *Langmuir,* 20: 6549-6555.
2. Martin, J. I., Wang, Z. G., Shick, M., (1996). "Effects of polymer brush self-assembly on spreading and thin film stability," *Langmuir,* 12: 4950-4959.
3. Reiter, G., Auroy, P., Auvray, L., (1996). "Instabilities of thin polymer films on layers of chemically identical grafted molecules," *Macromolecules,* 29: 2150-2157.
4. Ito, Y., Park, Y. S., Imanishi, Y., (1997). "Visualization of critical pH-controlled gating of a porous membrane grafted with polyelectrolyte brushes," *J. Am. Chem. Soc.,* 119: 2739-2740.
5. Ionov, L., Zdyrko, B., Sidorenko, A., Minko, S. Klep, V., Luzinov, I., Stamm, M., (2004). "Gradient polymer layers by "grafting to" approach," *Macromol. rapid comm.,* 25: 360-365.
6. Johnson, P. A., Gaspar, M. A., Levicky, R., (2004). "Polymer-anchored DNA gene monolayers," *J. Am. Chem. Soc.,* 126: 9910-9911.
7. Nakashima, H., Furukawa, K., Ajito, K., Kashimura, Y., Torimitsu, K., (2005). "Selective chemisorption of end-functionalized conjugated polymer on macro-and nanoscale surfaces," *Langmuir,* 21: 511-515.
8. De Bore, B., Simon, H. K., Werts, M. P. L., van der Vegte, E. W., Hadziioannou, G., (2000). "Living free radical photopolymerization initiated from surface-grafted iniferter monolayers," *Macromolecules,* 33: 349-356.
9. Weck, M., Jackiw, J. J., Rossi, R. R., Weiss, P. S., Grubbs, R. H., (1999). "Ring-opening metathesis polymerization from surfaces," *J. Am. Chem. Soc.,* 121: 4088-4089.
10. Hertler, W. R., Sogah, D. Y., Boettcher, F. P., (1990). "Group-transfer polymerization on a polymeric support," *Macromolecules,* 23: 1264-1268.
11. Abbasian, M., Jaymand, M., Ghadami, M. Z., Fathi, A., (2010). "Preparation of Reactive and Thermal Stable Hyperbranched Graft Copolymers/ Clay Nanocomposite via 'Living' Free Radical Polymerization," *Int. J. Nanosci. Nanotechnol.,* 6: 168-178.
12. Chen, W. Y., Zheng, J. X., Cheng, S. Z. D., Li, C. Y., Huang, P., Zhu, L., Xiong, H., Ge, Q., Guo, Y., Quirk, R. P., Lotz, B., Deng, L., Wu, C., Thomas, E. L., (2004). "Onset of tethered chain overcrowding," *Phys. rev. lett.,* 93: 028301-4.
13. Zheng, J. X., Xiong, H., Chen, W.Y., Lee, K., Van Horn, R. M., Quirk, R. P., Lotz, B., Thomas, E. L., Shi, A. -C., Cheng, S. Z. D., (2006). "Onsets of tethered chain overcrowding and highly stretched brush regime via crystalline-amorphous diblock copolymers," *Macromolecules,* 39: 641-650.
14. Xiong, H., Zheng, J. X., Van Horn, R. M., Jeong, K. -Un., Quirk, R. P., Lotz, B., Thomas, E. L., Brittain, W. J., Cheng, S. Z. D., (2007). "A new approach in the study of tethered diblock copolymer surface morphology and its tethering density dependence," *Polymer,* 48: 3732-3738.

15. Agbolaghi, S., Abbasi, F., Abbaspoor, S., Alizadeh-Osgouei, M., (2014). "Self-designed surfaces via single-co-crystallization of homopolymer and diblock copolymers in various growth conditions," *Eur. Polym. J.,* 66: 108–118.
16. Minko, S., Patil, S., Datsyuk, V., Simon, F., Eichhorn, K. -J., Motornov, M., Usov, D., Tokarev, I., Stamm, M., (2002). "Synthesis of adaptive polymer brushes via grafting to approach from melt," *Langmuir,* 18: 289-296.
17. Zhao, B., (2003). "Synthesis of binary mixed homopolymer brushes by combining atom transfer radical polymerization and nitroxide-mediated radical polymerization," *Polymer,* 44: 4079-4083.
18. Abbaspoor, S., Abbasi, F., Agbolaghi, S., (2014). "A novel approach to prepare polymer mixed-brushes via single crystal surface patterning," *RSC Adv.,* 4: 17071-17082.
19. Agbolaghi, S., Abbasi, F., Jalili, K., (2014). "Nascent lateral habits of solution crystallization of poly (ethylene glycol)-block-polystyrene diblock copolymers," *J Polym. Res.,* 21(380): 1-11
20. Agbolaghi, S., Abbasi, F., Abbaspoor, S., (2014). "Epitaxial single crystal surface patterning and study of physical and chemical environmental effects on crystal growth," *Colloid Polym. Sci.,* 292: 1375-1383.
21. Rahimi, K., Botiz, I., Stingelin, N., Kayunkid, N., Sommer, M., Koch, F. P., Nguyen, H., Coulembier, O., Dubois, P., Brinkmann, M., Reiter, G., (2012). "Controllable processes for generating large single crystals of poly(3-hexylthiophene)," *Angew. Chem. Int. Ed.,* 51: 11131-11135.
22. Wang, Y., Chen, J., Li, S., Li, L., Su, Q., Wang, J., Yang, X., (2011). "Semiconductor-insulator-semiconductor sandwiched lozenge crystals of poly(3-butylthiophene)-b-polyethylene copolymer," *Macromolecules,* 44: 1737-1741.
23. Nazari, M., Agbolaghi, S., Abbaspoor, S., Gheybi, H., Abbasi, F., (2016). "Arrangement of conductive rod nanobrushes via conductive–dielectric–conductive sandwiched single crystals of poly(ethylene glycol) and polyaniline block copolymers," *Macromolecules,* 48: 8947-8957.
24. Agbolaghi, S., Nazari, M., Abbaspoor, S., Gheybi, H., Abbasi, F., (2016). "Micro/nano conductive-dielectric channels designed by poly (ethylene glycol) single crystals covered by polyaniline nanofibers," *Polymer,* 92: 264-272.
25. Lotz, B., Kovacs, A. J., (1966). "Propriétés des copolymères biséquencés polyoxyéthylène-polystyrène," *Colloid Polym. Sci.,* 209(2): 97-114.
26. Lotz, B., Kovacs, A. J., Bassett, G. A., Keller, A., (1966). *Colloid Polym. Sci.,* 209: 115-128.
27. Agbolaghi, S., Abbasi, F. Abbaspoor, S., (2014). "Preparation of polymer brushes via growth of single crystals of poly (ethylene glycol)-block-polystyrene diblock copolymers synthesized by ATRP and studying the crystal lateral size and brush tethering density," *Polym. Bull.,* 71: 3177–3196.
28. Korayem, M. H., Karimi, A., Sadeghzadeh, S., (2014). "GDQEM Analysis for Free Vibration of V-shaped Atomic Force Microscope Cantilevers," *Int. J. Nanosci. Nanotechnol.,* 10: 205-214.
29. Korayem, A. H., Hoshiar, A. K., Badrlou, S., Korayem, M. H., (2016). "A Comprehensive Model for Stiffness Coefficients in V-Shaped Cantilevers," *Int. J. Nanosci. Nanotechnol.,* 12: 27-36.
30. Chen, W. Y., Li, C. Y., Zheng, J. X., Huang, P., Zhu, L., Ge, Q., Quirk, R. P., Lotz, B., Deng, L., Wu, C., Thomas, E. L., Cheng, S. Z. D., (2004). "Chemically shielded poly (ethylene oxide) single crystal growth and construction of channel-wire arrays with chemical and geometric recognitions on a submicrometer scale," *Macromolecules,* 37: 5292-5299.
31. Brandup, J., Immergut, E. H., (1975). "*Polymer Handbook*", New York: Wiley.
32. Richardson, P. H., Richard, R. W., Blundell, D. J., MacDonald, W. A., Mills, P., (1995). "Differential scanning calorimetry and optical microscopy investigations of the isothermal crystallization of a poly (ethylene oxide)-poly (methyl methacrylate) block copolymer," *Polymer,* 36: 3059-3069.
33. Wunderlich, B., (1973). "*Macromolecular physics*", Vol. 1: Crystal structure, morphology, defects, New York: Academic.